*Sensors and Materials*, Vol. 37, No. 5 (2025) 1871–1880
MYU Tokyo



S & M 4024

# Effects of Annealing on Properties of ITO:MgO/Ag Dual-layer Films for Sensor Material Applications

Cheng-Hsien Kuo,[1] Sigit Tri Wicaksono,[2] Shao-Tsen Wang,[3] and Tao-Hsing Chen[3*]

[1]Department of Die and Mold Engineering, National Kaohsiung University of Science and Technology, No. 415, Jiangong Rd., Sanmin Dist., Kaohsiung City 807618, Taiwan
[2]Department of Materials Engineering, Institut Teknologi Sepuluh Nopember (ITS), Surabaya 60111, Indonesia
[3]Department of Mechanical Engineering, National Kaohsiung University of Science and Technology, No. 415, Jiangong Rd., Sanmin Dist., Kaohsiung City 807618, Taiwan

(Received December 23, 2024; accepted April 21, 2025)

***Keywords:*** sputtering, ITO:MgO, annealing, transparent conducting film

In this study, we investigated the optical and electrical properties of ITO:MgO/Ag dual-layer transparent conducting films (with an atomic ratio of 97:3 at.%) annealed at different temperatures. Annealing was conducted in a vacuum utilizing thermal energy to rearrange the crystalline structure of the films, thus enabling atomic substitution, and to address internal defects. The optical and electrical properties of the dual-layer films were compared before and after annealing, revealing that the lowest resistivity of $2.92 \times 10^{-5}$ Ω·cm was in the unannealed state, the average transmittance was 58.97% at an annealing temperature of 500 °C, and the optimal figure of merit (FOM) was $7.71 \times 10^{-4}$ after annealing at a temperature of 300 °C.

## 1. Introduction

The advent of quantum mechanics has given rise to the energy band theory, which reveals the strong relationship between light and the energy gap of materials. This relationship suggests that changes in material properties can affect the energy gap.[1–3] Therefore, it caused many scientists to investigate how to obtain excellent optical properties of materials by changing the energy gap. Transparent conductive oxide (TCO) films, characterized by high conductivity and transparency, have been applied in various optical components including solar cells, flat-panel displays, thin-film transistors, and organic light-emitting devices.[4–8] A popular TCO thin film is ITO thin film; it has low resistivity that can be reduced to $1 \times 10^{-4}$ Ω·cm. Furthermore, it has a transmittance of more than 85%. However, the doped metal In of ITO is very rare. There are many reports on other high-optical-energy-gap and low-resistivity thin-film materials, such as ZnO, $In_2O_3$, $TiO_2$, $SnO_2$, and CdO, that can be used to replace ITO thin films.[9–13]

To achieve superior optical transmittance and electrical properties, recent studies have proposed oxide/metal dual-layer films that suppress the reflection of the intermediate metallic layer in the visible light range, thereby enhancing transmittance.[14–16]

*Corresponding author: e-mail: thchen@nkust.edu.tw
https://doi.org/10.18494/SAM5512

ISSN 0914-4935 
https://myukk.org/

In this study, dual-layer films were prepared by DC sputtering to deposit Ag as the metallic layer, followed by RF sputtering to deposit ITO:MgO as the oxide layer. Annealing was subsequently performed on the ITO:MgO/Ag dual-layer films before the sample thickness and electrical and optical properties, as well as their structural properties and surface morphologies, were evaluated. We hope that the dual-layer films can be used in optical sensor materials.

## 2. Materials and Methods

In this study, DC reactive magnetron sputtering was performed on a 99.99% pure metal (Ag) and ITO:3 at.% MgO ceramic target to fabricate Ag and ITO:MgO films. During the sputtering, the vacuum chamber pressure was controlled at 6 mTorr, the distance between the target and the glass substrate was set to 50 mm. The substrate was cleaned for 15–20 min in an ultrasonic bath using acetone and ethanol solutions, rinsed with deionized water, and dried with a high-purity $N_2$ flow. High-purity Ar gas (99.999%) was fed into the vacuum chamber with the total flow rate fixed at 15 sccm to deposit films with high transmittance and low resistivity. The ITO:MgO film was deposited for 30 min, with the sputtering power maintained at 80 W, and the Ag film was deposited for 1 min, with the sputtering power maintained at 20 W. The thickness of the sputtered films was measured using an α-step profiler, and their crystallinity was measured using an X-ray diffraction (XRD) system. Their surface morphologies were examined by AFM, and their optical transmittance was estimated using a spectrophotometer. Their electrical properties were measured using the AHM-800B Hall effect measurement system. Their optical properties were measured using a UV–VIS spectrometer (UV Solution 2900). Finally, their surface structure was examined by SEM (HITACHI SU-5000).

## 3. Results and Discussion

### 3.1 XRD analysis of film structure

Figure 1 shows the XRD spectra of the ITO:MgO/Ag films annealed at different temperatures, showing that the films remained amorphous in the unannealed state with no crystalline phases. Ag ions were uniformly distributed within the $In_2O_3$ lattice, indicating no distinct Ag peaks, and the ions began to crystallize after annealing at 200 ℃.

As the annealing temperature increased to 300 ℃, all the deposited samples contained only the $In_2O_3$ phase, exhibiting a polycrystalline cubic bixbyite structure with high-intensity diffraction, as seen in Fig. 1, indicating that tin atoms may have been substitutionally doped into the $In_2O_3$ lattice.[17] The amorphous ITO film exhibited a slight secondary diffusion bump at $2\theta \approx 30.5°$, while the peak near 38° corresponded to the Ag (411) plane.[18] The film was crystallized at 150–200 ℃, although the crystallization was relatively slow and incomplete with an annealing temperature of 200 ℃.[19] As the annealing temperature increased, the intensity of the main diffraction peak (222) significantly increased on the film surface; therefore, the dual-layer film became completely polycrystalline after annealing at temperatures of 300 and 400 ℃. As a result, the fully annealed ITO layer only exhibited a (222) preferential orientation because postannealing enhanced the intensity of the (222) diffraction peak.[20]

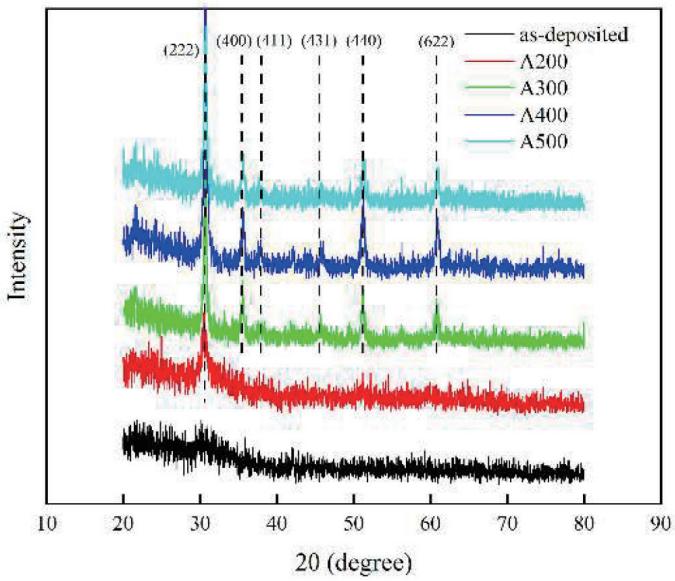


Fig. 1. (Color online) XRD spectra of ITO:MgO/Ag films after annealing at different temperatures.

Crystalline phases began to form when the ITO:MgO/Ag films were annealed at 300 °C, with peaks observed at 30.59, 35.46, 37.69, 45.69, 51.02, and 60.67 °C corresponding to the (222), (400), (411), (431), (440), and (622) planes, respectively. All peaks belonged to the $In_2O_3$ lattice, indicating that Ag ions may have been substituted into the lattice. The (222) peak was the primary growth orientation, with the peak intensity reaching its maximum at an annealing temperature of 400 °C as the temperature continued to increase.

### 3.2 Electrical properties at different annealing temperatures

The electrical properties of ITO:MgO/Ag films, which were measured using the Hall effect measurement system, are described in Table 1. The films exhibited the lowest resistivity of $2.92 \times 10^{-5}$ Ω·cm in the unannealed state, and their resistivity slightly increased with the annealing temperature but remained at $10^{-5}$ Ω·cm because annealing allowed the doped silver to diffuse into the oxide layer, facilitating substitutional mixing. However, the resistivity increased with the annealing temperature, leading to a degradation in electrical performance, probably because grain alignment and growth were both inhibited as the temperature approached the phase transformation point.

Further analysis of the XRD results suggested that the ITO:MgO/Ag films were amorphous in the unannealed state because the grains within the films may have continued growing. Moreover, when the annealing temperature reached 200 °C and the peak corresponding to $In_2O_3$ appeared, the resistivity increased to $3.37 \times 10^{-5}$ Ω·cm, largely owing to changes in carrier concentration. The resistivity further increased to $4.82 \times 10^{-5}$ Ω·cm as the temperature rose to 400 °C but decreased when the temperature reached 500 °C.

Table 1
Electrical properties of ITO:MgO/Ag films after annealing at different temperatures.

| ITO:MgO (80 W, 30 min) / Ag (20 W, 1 min) | | | |
|---|---|---|---|
| Annealing temperature (°C) | Resistivity (Ω·cm) | Mobility ($cm^2/Vs$) | Carrier concentration ($cm^{-3}$) |
| As-deposited | $2.92 \times 10^{-5}$ | $9.00 \times 10^{0}$ | $1.41 \times 10^{21}$ |
| 200 | $3.37 \times 10^{-5}$ | $8.78 \times 10^{0}$ | $2.11 \times 10^{22}$ |
| 300 | $3.83 \times 10^{-5}$ | $1.26 \times 10^{1}$ | $5.01 \times 10^{21}$ |
| 400 | $4.82 \times 10^{-5}$ | $2.60 \times 10^{1}$ | $9.11 \times 10^{21}$ |
| 500 | $4.67 \times 10^{-5}$ | $1.53 \times 10^{1}$ | $8.76 \times 10^{21}$ |

Table 2
Energy gap of ITO:MgO/Ag films after annealing at different temperatures.

| Energy gap (eV) | |
|---|---|
| Annealing temperature (°C) | 80 W for 30 min |
| As-deposited | 3.45 |
| 200 | 3.42 |
| 300 | 3.61 |
| 400 | 3.63 |
| 500 | 3.71 |

### 3.3 Optical properties after annealing

Table 2 and Fig. 2 show the changes in the energy gap and optical properties of the dual-layer films after annealing, respectively, which indicate that the average transmittance at the metallic layer was 56–58%. The transmittance showed a slight increase across the board as the annealing temperature increased. The optical energy gap (*Eg*) was calculated as[21–23]

$$(\alpha h\upsilon)^2 = A(h\upsilon - Eg), \tag{1}$$

where $A$ is a constant, and $\alpha$ and $h\upsilon$ are the absorption coefficient and incident photon energy, respectively. There is a linear relationship between $(\alpha h\upsilon)^2$ and $h\upsilon$, which can be used to estimate *Eg*. The energy gap was 3.45 eV before annealing (at 80 W for 30 min) but reached its maximum of 3.71 eV after annealing at 500 °C. The average transmittance showed no significant changes, and there were no notable changes in energy gap. Overall, the energy gap of the films met the criteria for the fabrication of wide-bandgap semiconductors.

### 3.4 Surface morphology before and after annealing

Figure 3 shows that the surface morphology of the ITO:MgO/Ag films became smoother and denser as the annealing temperature increased. The surface roughness (*Ra*) values obtained by AFM were less than 10 nm (Table 3), indicating that the dual-layer films had a highly smooth surface. Moreover, *Ra* decreased as the annealing temperature increased, suggesting that annealing effectively reduced the *Ra* of the films. This was mainly because the crystallization of

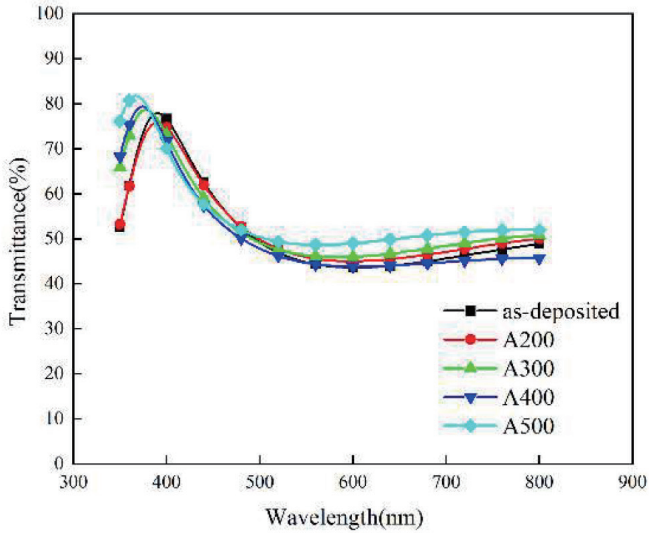


Fig. 2. (Color online) Transmittance of ITO:MgO/Ag films after annealing at different temperatures.

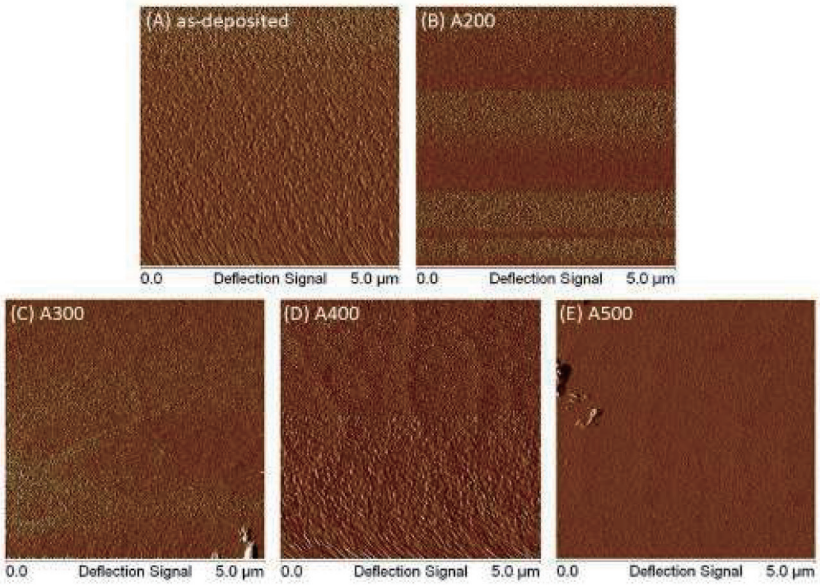


Fig. 3. (Color online) Two-dimensional AFM visualization of surface morphology when ITO:MgO/Ag films were (a) deposited and annealed at (b) 200, (c) 300, (d) 400, and (e) 500 °C.

Table 3
Surface roughness of ITO:MgO/Ag films crystallized after annealing at different temperatures.

| Annealing temperature (°C) | *Ra* (nm) |
|---|---|
| 200 | 10.1 |
| 300 | 8.57 |
| 400 | 5.21 |
| 500 | 1.32 |

ITO:MgO after rearrangement led to a reduction in *Ra*, resulting in a denser and smoother surface, and the roughness began to decrease after annealing. The surface morphology of the films was subsequently analyzed by SEM, as shown in Fig. 4, revealing that the energy provided during annealing facilitated Ag precipitation on the film surface, promoting the formation of Ag nanoparticles.

### 3.5 Grain size

The grain size of the ITO:MgO/Ag films was estimated using the Scherrer equation, which took into account the main XRD peak, as follows:[24]

$$D = \frac{0.9\lambda}{\beta \cos\theta}, \tag{2}$$

where $D$ is the grain size, $\lambda$ is the incident wavelength of the X-ray, $\lambda = 0.15418$ nm, $\theta$ is the angle of incidence, and $\beta$ is the full width at half-maximum (FWHM). Both $\lambda$ and $\theta$ are constants; therefore, $D$ is inversely proportional to $\beta$, that is, the grain size increases as FWHM decreases.[25] The values for $\theta$ and $\beta$ were obtained by substituting the data into the equation.

Figure 5 shows changes in the grain size and FWHM of ITO:MgO/Ag films after annealing. The crystalline phases of the films began to form at the annealing temperature of 200 ℃, at which point the smallest grain size was observed. Notably, FWHM decreased when the annealing temperature increased to 300 ℃, but it improved with an increase in temperature, leading to gradual decreases in grain size from 23.97 to 23.36 nm. To present the change in FWHM with grain size, Table 4 shows the FWHM values and grain sizes shown in Fig. 5.

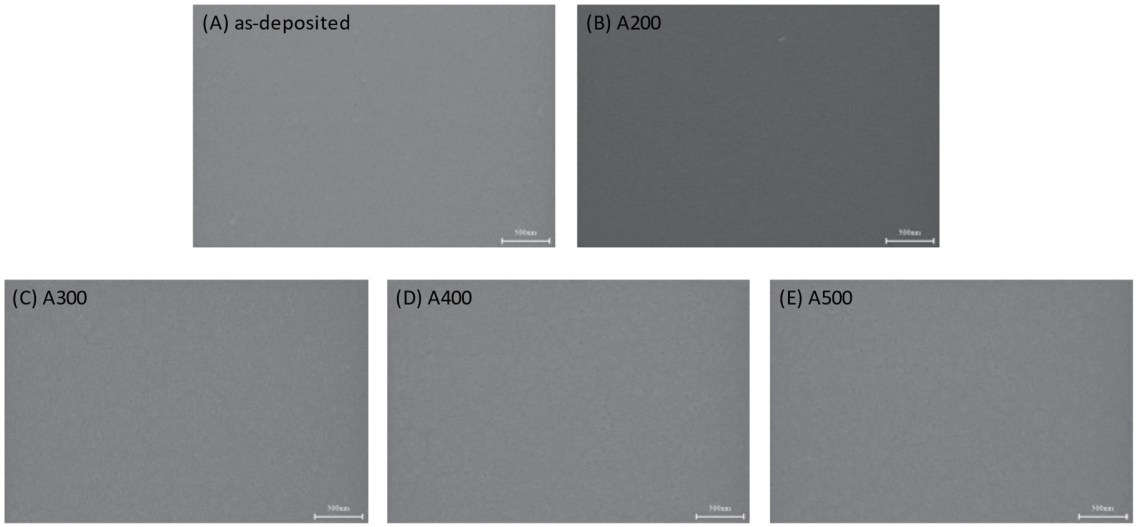


Fig. 4. (Color online) SEM visualization of surface morphology when ITO:MgO/Ag films were (a) deposited and annealed at (b) 200, (c) 300, (d) 400, and (e) 500 ℃.

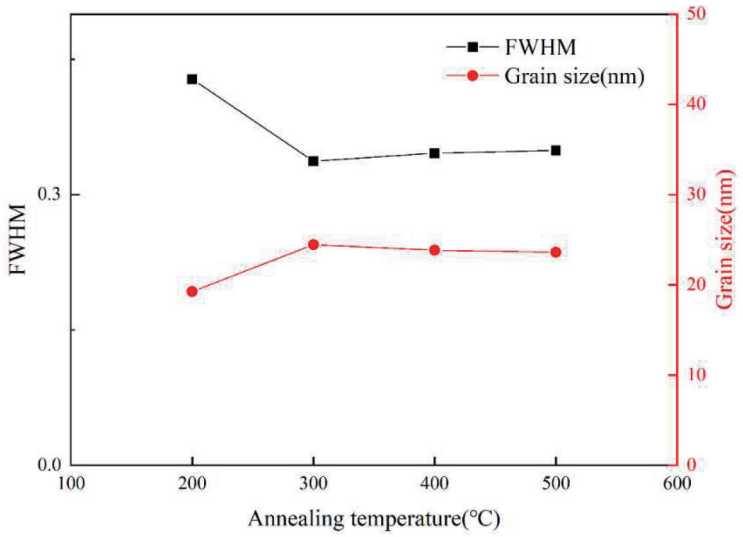


Fig. 5. (Color online) Grain sizes of ITO:MgO/Ag films annealed at different temperatures.

Table 4
FWHM values and grain sizes in Fig. 5.

| ITO:MgO/Ag (80 W for 30 min) | | |
|---|---|---|
| Annealing temperature (°C) | FWHM | Grain size (nm) |
| 200 | 0.387 | 21.30 |
| 300 | 0.344 | 23.97 |
| 400 | 0.378 | 21.81 |
| 500 | 0.373 | 22.16 |

### 3.6 Figure of merit (FOM) values obtained before and after annealing

FOM is used to evaluate the material quality of transparent conducting films. In this study, the FOM values of the dual-layer films at different annealing temperatures were determined in terms of resistivity and transmittance as follows:[26]

$$\varnothing_{TC} = \frac{T_{av}^{10}}{R_{sh}}, \tag{3}$$

where $T_{av}$ is the average optical transmittance and $R_{sh}$ is the sheet resistance (expressed in units of $\Omega^{-1}$). The equation suggests that FOM is proportional to the 10th power of transmittance; thus, transmittance significantly affects FOM. Films must exhibit a higher transmittance and a lower resistivity to achieve a more satisfactory FOM. Figure 6 depicts changes in FOM for ITO:MgO/Ag films after annealing at different temperatures. The optimal FOM of $7.71 \times 10^{-4}$ $\Omega^{-1}$ was obtained at 300 °C, mainly because of excellent electricity conductivity achieved at this annealing temperature. Table 5 presents the FOM and sheet resistance values and their relationship with annealing temperature.

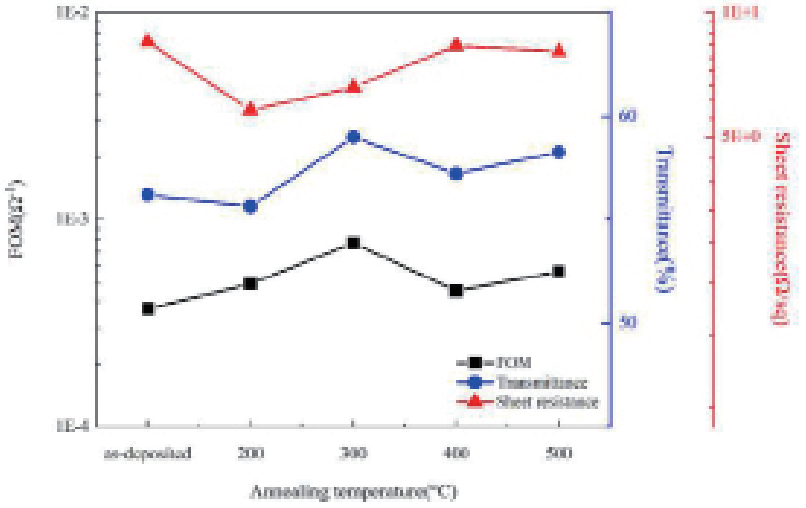


Fig. 6. (Color online) FOM values of ITO:MgO/Ag films after annealing at different temperatures.

Table 5
FOM and transmittance values shown in Fig. 6.

| Annealing temperature (°C) | FOM, $\varnothing_{TC}$ ($\Omega^{-1}$) | Transmittance (%) |
|---|---|---|
| As-deposited | $3.70 \times 10^{-4}$ | 56.19 |
| 200 | $4.89 \times 10^{-4}$ | 55.63 |
| 300 | $7.71 \times 10^{-4}$ | 56.9 |
| 400 | $4.52 \times 10^{-4}$ | 57.20 |
| 500 | $5.6 \times 10^{-4}$ | 58.97 |

## 4. Conclusions

The XRD analysis revealed that the films were amorphous in the unannealed state, but crystalline phases appeared after annealing at a temperature of 200 °C. Distinct $In_2O_3$ peaks were observed when the annealing temperature increased to 300 °C, indicating that Ag ions were substitutionally doped into the $In_2O_3$ lattice, with the (222) peak being the primary growth orientation. The peak intensity reached its maximum when the annealing temperature increased to 400 °C. Regarding their electrical properties, the films exhibited the lowest resistivity of $2.92 \times 10^{-5}$ Ω·cm in the unannealed state, with the highest average transmittance (58.97%) and maximum energy gap (3.71 eV) observed after annealing at a temperature of 500 °C.

The *Ra* of the films was less than 14 nm at all the annealing temperatures tested, indicating a highly smooth surface. Moreover, the roughness decreased as the annealing temperature increased, suggesting that annealing helps to reduce film roughness, a phenomenon subsequently confirmed by SEM analysis. Regarding the changes in the grain size of the films after annealing, crystalline phases began to form at an annealing temperature of 200 °C. This tendency was consisted with the XRD result of a high intensity diffraction value after annealing at a

temperature of 200 °C. However, the optimal FOM of the films was observed at $7.71 \times 10^{-4}\,\Omega^{-1}$ after annealing at a temperature of 300 °C. The ITO:MgO/Ag dual-layer films have good electrical conductivity with appropriately high transmission in the near-VIS region. According to the results, ITO:MgO/Ag dual-layer films can be applied to optical sensor materials owing to their excellent optical and electrical properties.

## Acknowledgments

This study was conducted under the Research Project MOST111-2628-E-992-001-MY2, which was supported by the National Science and Technology Council of Taiwan. We would like to express our gratitude to the National Science and Technology Council for its support, which enabled the smooth completion of this research. We also gratefully acknowledge the use of EM000700 of MOST 110-2731-M-006-001, which belongs to the Core Facility Center of National Cheng Kung University.

## References

1 A. N. Banerjee and K. K. Chattopadhyay: Prog. Cryst. Growth Charact. Mater. **50** (2005) 52. https://doi.org/10.1016/j.pcrysgrow.2005.10.001
2 O. Sanchez-Sobrado, M. J. Mendes, T. Mateus, J. Costa, D. Nunes, H. Aguas, E. Fortunato, and R. Martins: Solar Energy **195** (2020) 92. https://doi.org/10.1016/j.solener.2019.11.051
3 H. G. Park, S. Q. Hussain, J. Park, and J. Yi: J. Mater. Sci. **59** (2024) 13873. https://doi.org/10.1007/s10853-024-09506-7
4 K. Kacha, F. Djeffal, H. Ferhati, L. Foughali, A. Bendjerad, A. Benhaya, and A. Saidi: Ceram. Int. **47** (2021) 2019. https://doi.org/10.1016/j.ceramint.2022.03.298. https://doi.org/10.1016/j.ceramint.2022.03.298
5 C. Wang, D. Zhuang, M. Zhao, Y. Li, L. D, H. Wang, J. Wai, and Q. Gong: Ceram. Int. **47** (2022) 34508. https://doi.org/10.1016/j.ceramint.2021.08.365
6 A. A. Rakesh, S. Nallin, S. Maheshwar, and S. Madhuri: Rev. Adv. Mater. Sci. **53** (2018) 79. https://doi.org/10.1515/rams-2018-0006
7 K Natu, M Laad, B Ghule, and A Shalu: J. Appl. Phys. **34** (2023) 190701. https://doi.org/10.1063/5.0169308
8 S. K. Preeti: Sol. Energy Mater. Sol. Cells **48** (2022) 20194.
9 Z. El Hafidi, N. Outaleb, and Y. Naimi: J. Mater. Sci.-Mater. Electron. **35** (2024) 1861. https://doi.org/10.1007/s10854-024-13623-z
10 T. H. Chen, T. C. Cheng, and Z. R. Hu: Microsyst. Technol. **19** (2013) 1787. https://doi.org/10.1007/s00542-013-1837-5
11 J. Müller, B. Rech, J. Springer, and M. Vanecek: Sol. Energy **77** (2004) 917. https://doi.org/10.1016/j.solener.2004.03.015.
12 T. H. Chen and C. L. Yang: Opt. Quantum Electron. **48** (2016) 533. https://doi.org/10.1007/s11082-016-0808-3.
13 A. Dalal, M. Mishra, S. Chakrabarti, R. K. Gupta, and A. Mondal: Vaccum **201** (2022) 111115.
14 T. Y. Tsai, C. J. Liu, T. D. Chang, S. L. Tu, and T. H. Chen: Sens. Mater. **36** (2024) 671. https://doi.org/10.18494/SAM4684 https://doi.org/10.1016/j.vacuum.2022.111115
15 M. Y. Yen, T. H. Chen, P. H. Lai, S. L. Tu, and Y. H. Shen: Sens. Mater. **33** (2021) 3941. https://doi.org/10.18494/SAM.2021.3706
16 H. Ferhati and F. Djeffal: J. Comput. Electron. **19** (2020) 815. https://doi.org/10.1007/s10825-020-01459-9
17 M. Gulen, G. Yildirim, S. Bal, A. Varilci, I. Belenli, and M. Oz: J. Materi. Sci. Materi. Electron. **24** (2013) 467.
18 T. H. Chen and T. Y. Chen: Nanomaterials **5** (2015) 1831. https://doi.org/10.3390/nano5041831
19 C. F. Liu, T. H. Chen, and J. T. Huang: Sens. Mater. **32** (2020) 3727. https://doi.org/10.18494/SAM.2020.3138
20 B. Zhang, X. Dong, X. Xu, X. Wang, and J. Wu: Mater. Sci. Semicond. Process. **10** (2007) 264. https://doi.org/10.1016/j.mssp.2008.03.003Get rights and content
21 C. F. Liu, C. H. Kuo, T. H. Chen, and Y. S. Huang: Coatings **10** (2020) 394. https://doi.org/10.3390/coatings10040394

22 M. Micali, S. Cosentino, and A. Terrasi: Sol. Energy Mater. Sol. Cells **221** (2021) 110904. https://doi.org/10.1016/j.solmat.2020.110904
23 J. W. Jeong, H. Kong, and H. Y. Lee: Superlattices Microst. **133** (2019) 106178. https://doi.org/10.1016/j.spmi.2019.106187
24 B. D. Cullity and S. R. Stock: Elements of X-ray Diffraction (Prentice Hall, 2001), Chap. 5-2, pp. 167–171.
25 C. F. Liu, T. H. Chen, and Y. S. Huang: Sens. Mater. **32** (2021) 2321. https://doi.org/10.18494/SAM.2020.2867
26 B. Sarma, D. Barman, and B. K. Sarma: Appl. Surf. Sci. **479** (2019) 786. https://doi.org/10.1016/j.apsusc.2019.02.146.

## About the Authors

**Cheng-Hsien Kuo** received his Ph.D. degree in mechanical engineering from National Yang Ming Chiao Tung University, ROC. He is currently an associate professor in the Department of Mold and Die Engineering at National Kaohsiung University of Science and Technology. His research interests include CAD/CAM/CAE, batteries, solar cells, electrical sensors, and the joining of dissimilar materials.

**Sigit Tri Wicaksono** received his B.S. and M.S. in physics science from the Faculty of Natural Sciences, Institute Teknologi Sepuluh Nopember (ITS), Indonesia. He obtained his Ph.D. degree in materials science and engineering from National Taiwan University of Science and Technology (NTUST), Taiwan. He has been a professor in the Department of Materials Engineering, ITS, Surabaya, Indonesia. His research interests are in composite materials, thin-film materials, and sensors.

**Shao-Tsen Wang** received his B.S. degree from National Kaohsiung University of Science and Technology, Taiwan, where he is currently studying for his M.S. degree. His research interests are in TCO thin films, materials engineering, and sensors.

**Tao-Hsing Chen** received his B.S. degree from National Cheng Kung University, Taiwan, in 1999 and his M.S. and Ph.D. degrees from the Department of Mechanical Engineering, National Cheng Kung University, in 2001 and 2008, respectively. From August 2008 to July 2010, he was a postdoctoral researcher at the Center for Micro/Nano Science and Technology, National Cheng Kung University. In August 2010, he became an assistant professor at National Kaohsiung University of Applied Sciences (currently National Kaohsiung University of Science and Technology), Taiwan. Since 2016, he has been a professor at National Kaohsiung University of Science and Technology. His research interests are in metal materials, TCO thin films, thermal sensors, and photosensors. (thchen@nkust.edu.tw)